Sensors & Actuators: B. Chemical 291 (2019) 319–328

Contents lists available at ScienceDirect

Sensors and Actuators B: Chemical

journal homepage: www.elsevier.com/locate/snb

Cobalt-based metal-organic frameworks as co-reaction accelerator for enhancing electrochemiluminescence behavior of *N*-(aminobutyl)-*N*-(ethylisoluminol) and ultrasensitive immunosensing of amyloid-β protein

Chao Wang[a], Nuo Zhang[a], Yueyuan Li[a], Lei Yang[a], Dong Wei[b], Tao Yan[b], Huangxian Ju[c], Bin Du[b], Qin Wei[a,*]

[a] Key Laboratory of Interfacial Reaction & Sensing Analysis in Universities of Shandong, School of Chemistry and Chemical Engineering, University of Jinan, Jinan, 250022, PR China
[b] School of Resources and Environment, University of Jinan, Jinan, 250022, PR China
[c] State Key Laboratory of Analytical Chemistry for Life Science, School of Chemistry and Chemical Engineering, Nanjing University, Nanjing, 210023, PR China

ARTICLE INFO

Keywords:
Electrochemiluminescence immunosensor
N-(Aminobutyl)-*N*-(ethylisoluminol)
Co-reaction accelerator
Metal-organic frameworks
Amyloid-β protein

ABSTRACT

In this work, a "luminophore/coreactant/co-reaction accelerator" ternary electrochemiluminescence (ECL) system is proposed by using *N*-(aminobutyl)-*N*-(ethylisoluminol) (ABEI) functionalized cobalt-based MOFs (Co-MOFs/ABEI) with superior peroxidase-like activities as the luminophore. ABEI, the derivative of luminol, is used as the reductant and organic ligand to synthesize flower-like Co-MOFs/ABEI. The as-synthesized Co-MOFs/ABEI not only function as desirable nano-carriers for the enrichment of ABEI, but also act as co-reaction accelerators for the catalysis of H_2O_2 decomposition. Furthermore, Au nanoparticles are decorated on Co-MOFs/ABEI via electrostatics attraction, endowing it with favorable biocompatibility and electrocatalytic property to bond with detection antibodies and generate more excited state ABEI*. Besides, with the advantages of large specific surface area and easy preparation, Au nanoparticles functionalized Fe_3O_4@polypyrrole is utilized to anchor the capture antibodies for immunoaction with target analyte. Amyloid-β protein ($A\beta_{42}$), a principal hallmark of Alzheimer's disease, is chosen as the target analyte. The proposed $A\beta_{42}$ immunosensor performs with a broad linear range from 10 fg mL^{-1} to 100 ng mL^{-1} and a detection limit down to 3 fg mL^{-1}, opens up new prospects for clinical analysis of $A\beta_{42}$ and provides promising approaches to synthesize luminophore-functionalized MOFs with high luminous efficiency for ECL bioanalysis.

1. Introduction

Population aging, a global hotspot in the 21st century, has brought about an urgent issue that every nation must concern: Alzheimer's disease (AD). AD is a severe neurodegenerative disorder of brain, which is caused by the deposition and accumulation of amyloid-β protein (Aβ, with a molecular weight about 4 kDa and 39–43 amino acid residues in lengths) in the brain [1]. The predominant components of Aβ exist in two forms: 40-amino-acid-peptide ($A\beta_{40}$) and 42-amino-acid-peptide ($A\beta_{42}$). Compared with $A\beta_{40}$, $A\beta_{42}$ has two additional residues at the carboxyl-terminal of $A\beta_{40}$ with a greater propensity towards self-aggregation into plagues, thus it is the principal species deposited within the parenchyma of AD brain. Of the monomeric, oligomeric and fibrillar forms of $A\beta_{42}$, a mass of evidences indicate that soluble $A\beta_{42}$ oligomers are the major neurotoxic species in AD, thus $A\beta_{42}$ oligomers have been exploited as reliable and predictive biomarkers of AD [2]. Recent insights have demonstrated that increases of the $A\beta_{42}$ plague concentration inside the brain's cells or decreases of the $A\beta_{42}$ concentration in serum indicate the onset of AD [3]. The challenge of $A\beta_{42}$ detection in serum is how to reduce the detection limit as low as possible since the $A\beta_{42}$ levels in the serum of AD subjects could be detected from 25 to 85 pg mL^{-1} [4,5]. Therefore, it is of great significant to employ predominant analytical methods and effective signal amplification strategies for the ultrasensitive analysis of $A\beta_{42}$. Towards this direction, there is a growing body of literature about the detection of $A\beta_{42}$, including fluorescence [6], electrochemical [7], photoelectrochemical [8], localized surface plasmon resonance (LSPR) [9] and so on. Among these analytical methods, electrochemiluminescence (ECL), which integrates the merits of chemiluminescence and electrochemistry, possesses overwhelming popularity in view of its extraordinary properties such as

* Corresponding author.
E-mail address: sdjndxwq@163.com (Q. Wei).

https://doi.org/10.1016/j.snb.2019.04.097
Received 4 January 2019; Received in revised form 16 April 2019; Accepted 18 April 2019
Available online 18 April 2019
0925-4005/

superb sensitivity, simplified device and excellent controllability [10,11].

As the most conventional ECL reagents, luminol and its derivatives have triggered off tremendous attention on account of their low oxidation potential, high luminous efficiency and nontoxicity [12,13]. Notably, as a special analogue of luminol, *N*-(aminobutyl)-*N*-(ethylisoluminol) (ABEI) could be functionalized with nanomaterials more easily than luminol because it possesses an extra active primary amino away from the conjugated attraction of the aromatic ring [14]. In an effort to boost the ECL efficiency of ABEI and enhance the detection sensitivity, lately, Yuan's group reported that by introducing a co-reaction accelerator into the luminophore-coreactant system, the ECL response of luminophore could be enhanced remarkably [15]. The co-reaction accelerator is supposed to be a species that could react with coreactant rather than the luminophore to fasten the electrochemical reaction of coreactant for generating more active intermediates, thus achieving the ECL signal amplification [16]. Specifically, employing peroxidase or peroxidase mimics as the co-reaction accelerator towards H_2O_2 could speed up the decomposition of H_2O_2 to produce plentiful reactive oxygen species (ROSs) like superoxide radical ($O_2^{\cdot -}$) and hydroxyl radical ($OH^{\cdot}$) [17], which could further react with ABEI for reaction efficiency improvement.

Up to now, thanks to the high stability against pH and temperature as well as desirable enzyme-mimicking activity of peroxidase mimics, great advances have been made in the application of peroxidase mimics in the luminophore/coreactant/co-reaction accelerator ternary system, such as MoS_2 nanoflowers [18], CuS nanosphere [19] and V_2O_5 nanospheres [20]. Nonetheless, the reported immobilization methods of ABEI still encounter the drawbacks of finite loading capacity and cumbersome preparation process because ABEI was merely coexisted on the surface of peroxidase mimics via weak covalent interactions. Hence, the research on efficient strategies to load ABEI abundantly on nanomaterials is a challenge and persistent theme in the field of ECL. Metal-organic frameworks (MOFs), which consist of metal centers or clusters and organic bridging ligands, have emerged as attractive research targets owing to the intriguing features of excellent chemical tailorability, high specific surface area and desirable thermal stability [21,22]. Such a hybrid opens an attractive class of highly efficient loading of luminophore on nanomaterials for ECL enhancement [23]. For instance, a competitive ECL biosensor was constructed by using Ru $(bpy)_3^{2+}$ encapsulated in UiO-67 as the luminophor for the diethylstilbestrol detection [24]. By using Fe-MIL-101 as the scaffold of ABEI, Jiang synthesized a novel ECL signal probe which combined the luminophor and MOFs in one molecule and applied it to the sensitive bioassay of mucin1 [25]. Moreover, Yang designed an electrochemical aptasensor by employing the electroactive Co-MOFs/PtPd nanoparticles as the peroxidase mimics for electrochemical signal amplification [26]. However, the investigation on Co-based MOFs as the nanocarriers of ABEI is still in its infancy.

Inspired by these intellectual reports, in this study, novel flower-like ABEI functionalized cobalt-based MOFs (Co-MOFs/ABEI) were synthesized via utilizing ABEI crosslinked 2-aminoterephthalic acid (NH_2-BDC) as the organic bridging ligand and ABEI as the reductant. Furthermore, benefited from the admirable biocompatibility and favorable catalytic property, Au nanoparticles (Au NPs) were decorated on the Co-MOFs/ABEI by electrostatic attraction to form Co-MOFs/ABEI-Au nanocomposites, thus more stable and enhanced ECL signals were achieved. The as-prepared Co-MOFs/ABEI not only acted as desirable nanocarriers for the enrichment of ABEI, but also exhibited satisfying peroxidase mimics properties for the catalysis of H_2O_2 decomposition. Meanwhile, the immunosensing platform plays a crucial role in the sensitivity improvement of immunosensor. Recently, transition metal oxides [27–29] and carbon-based materials [30–32] with enormous specific surface area and intrinsic electroconducitivity have been extensively applied as electrochemical mediator. In this work, Au NPs decorated Fe_3O_4@polypyrrole (Fe_3O_4@PPy-Au) with the merits of desirable biocompatibility and easy of magnetic separation was chosen as the immunosensing platform to immobilize the capture antibody (Ab_1).

Based on the mentioned above, an ultrasensitive ECL immunosensor was fabricated by employing Co-MOFs/ABEI-Au with high luminous efficiency and stable luminous ability as an ideal signal probe for the trace determination of $A\beta_{42}$. Incremental ECL intensities were attained accordingly with the increasing of $A\beta_{42}$ concentrations from 10 fg mL^{-1} to 100 ng mL^{-1}, and the detection limit was as low as 3 fg mL^{-1}. This novel solid-state ECL ternary platform introduced Co-MOFs as the coreaction accelerator for H_2O_2 decomposition, which not only met the requirement of quantitative determination of $A\beta_{42}$, but also offered an effective means to synthesize highly efficient ABEI-based nanomaterials and widened the application range of ABEI in ECL field. With excellent stability, outstanding selectivity and satisfying reproducibility, the proposed immunosensor could be applied as a powerful tool to detect a series of biomarkers, revealing it great potential in the clinical diagnosis and real-time monitoring for AD.

2. Experimental section

2.1. Materials

Cobaltous nitrate ($Co(NO_3)_2{\cdot}6H_2O$), ferric chloride hexahydrate ($FeCl_3{\cdot}6H_2O$), sodium acetate (NaAc), 2-aminoterephthalic acid (NH_2-BDC) and glutaraldehyde (GA, 50%) were bought from China Medicine Group Shanghai Chemical Reagent Corporation. Poly diallyldimethylammonium chloride (PDDA), polyethylene glycol (PEG), pyrrole, bovine serum albumin (BSA, 96–99%), gold chloride ($HAuCl_4{\cdot}4H_2O$), N, N-dimethylformamide (DMF) and *N*-(aminobutyl)-*N*-(ethylisoluminol) (ABEI) were purchased from Sigma-Aldrich (Beijing, China). Phosphate buffer saline (PBS) with different pH values were prepared with 0.1 M Na_2HPO_4, 0.1 M KH_2PO_4 and 0.1 M KCl. Ferricyanide solution ($Fe(CN)_6^{3-/4-}$, 5 mM) was made by $K_3[Fe(CN)_6]$ and $K_4Fe(CN)_6{\cdot}3H_2O$ dissolving with PBS (pH 7.4). Ultrapure water with an electrical resistance of 18.25 MΩ cm was used throughout all experiments. Amyloid-β protein ($A\beta_{42}$), amyloid-β protein capture antibody (Ab_1), detection antibody (Ab_2) and $A\beta_{40}$ were supplied by Nanjing Kingsrui Technology CO. LTD. The interferences of carcinoembryonic antigen (CEA), prostatic specific antigen (PSA), and carbohydrate antigen 125 (CA125) were provided by Shanghai Linc-Bio Science Co. LTD (Shanghai, China). All chemical reagents were analytical grade and directly used without further purification.

2.2. Preparation of Fe_3O_4@PPy-Au

Fe_3O_4 nanoparticles were synthesized as follows. Firstly, 0.005 mol of $FeCl_3{\cdot}6H_2O$ was dispersed in 40 mL of ethylene glycol. Then, 0.044 mol of sodium acetate (NaAc) and 1.0 g of polyethylene glycol were put in the above solution and blended for 0.5 h. Afterwards, the resultant solution was moved to a 50 mL of Teflon-lined stainless-steel autoclave and reacted at 200 °C for 8 h. After cooled down to 20 °C, Fe_3O_4 nanoparticles were acquired by magnetic separation and dried in vacuum. Fe_3O_4@PPy nanocomposites were prepared according to the report of Wang [33]. At first, 0.3 g of Fe_3O_4 nanoparticles were dissolved in 70 mL of ultrapure water. Then, 3 mL of pyrrole in 15 mL of alcohol and 15 mL of HCl (6 mol L^{-1}) were added in the above solution with ultrasonic treatment for 90 min. Lastly, Fe_3O_4@PPy nanocomposites were obtained by magnetic seperation and washed by ethanol and water for three times. For preparation of Fe_3O_4@PPy-Au, 1 mL of Fe_3O_4@PPy (10 mg mL^{-1}) was mingled with 40 mL of as-prepared Au NPs sol (the preparation details were shown in Supplementary material) and shook for 5 h. The Fe_3O_4@PPy-Au was obtained by magnetic separation and dried in vacuum.

2.3. Preparation of Co-MOFs/ABEI-Au-Ab_2 signal probe

The Co-MOFs/ABEI nanomaterial was synthesized according to previous method with some modification [26]. Typically, 0.0002 mol of ABEI and 0.0004 mol of NH_2-BDC were added into DMF (15 mL). Next, 1.0 mL of 1% glutaraldehyde was dropped into the mixture to crosslink NH_2-BDC and ABEI with magnetic stirring for 48 h under lucifugal situation. Afterwards, 0.0006 mol of $Co(NO_3)_2{\cdot}6H_2O$ was put into the mixture and heated in an oil bath at 140 °C for 4 h. The precipitation was obtained by centrifugation and rinsed two times with ethanol followed by drying at 60 °C. The Co-MOFs/ABEI-Au nanocomposites were obtained by electrostatic attraction. To begin with, 0.5 mL of PDDA was dropped into 3 mL of H_2O and ultrasonicated for 5 min. Then, 5 mg of Co-MOFs/ABEI was dissolved in the above solution with vibration for 12 h. The positively charged Co-MOFs/ABEI was procured by centrifugal separation and mixed with 10 mL of negatively charged Au NPs solution with shaking for another 12 h to get Co-MOFs/ABEI-Au. After centrifugation, 1 mL of $A\beta_{42}$ detection antibody (Ab_2, 1 μg mL^{-1}) was dropped into 1 mL of the synthesized Co-MOFs/ABEI-Au solution and reacted at 4 °C overnight. Finally, the Co-MOFs/ABEI-Au-Ab_2 bioconjugate was obtained via centrifugation and dispersed in 1 mL of PBS (pH 7.4), followed by adding 10 μL of BSA (1%) to block the nonspecific binding sites.

2.4. Fabrication of the sensing interface

The preparation process of different materials and the fabrication procedure of the $A\beta_{42}$ immunosensor were illustrated in Scheme 1. Initially, glassy carbon electrode (GCE, 4 mm in diameter) was polished with 0.3 μm and 0.05 μm of aluminum slurry to obtain a mirror-like surface and rinsed thoroughly with ultrapure water. Afterwards, 6 μL of prepared Fe_3O_4@PPy-Au (3 mg mL^{-1}) was coated on the polished electrode and dried naturally. Next, the modified GCE was incubated with 6 μL of $A\beta_{42}$ capture antibody (Ab_1, 10 μg mL^{-1}) for 12 h at 4 °C. After rinsing carefully with PBS (pH 7.4), 3 μL of BSA (1%) was pipetted on the GCE surface to preclude the possible nonspecific binding. 40 min later, the modified GCE was washed thoroughly with PBS (pH 7.4) and stored at 4 °C for the following measurement.

2.5. ECL detection of $A\beta_{42}$

The detection of $A\beta_{42}$ was based on sandwiched immunoreaction. At first, 6 μL of various concentrations of $A\beta_{42}$ antigens were bound on the abundant Ab_1 modified GCE. After washing the redundant antigens carefully, 6 μL of Ab_2 bioconjugates were incubated with $A\beta_{42}$ antigens for 40 min and rinsed with PBS (pH 7.4) carefully. Lastly, ECL responses of these modified electrodes were recorded with a MPI-F flow-injection chemiluminescence detector in 10 mL of PBS (pH 7.4) containing 10 μL of H_2O_2 under the potential scan from 0 V to 0.7 V with a scan rate of 0.1 V s^{-1}. The voltage of photomultiplier tube was set at 700 V. The ECL intensity was positively correlated with the concentration of $A\beta_{42}$, by which $A\beta_{42}$ could be detected sensitively.

3. Results and discussion

3.1. Characterizations of nanomaterials

The morphologies and sizes of the prepared nanomaterials were examined by scanning electron microscopy (SEM). As displayed in Fig. 1A, the Fe_3O_4 nanocrystal exhibited a typical nanosphere morphology with a smooth surface and a mean diameter of 220 nm. Fig. 1B presented that the Fe_3O_4 nanospheres were wrapped by polypyrrole (PPy) and the Fe_3O_4@PPy nanocomposites possessed a rugged surface, which could afford large surface area for the attachment of Au NPs via Au-N bond. As shown in Fig. 1C, abundant Au NPs were located evenly on the surface of Fe_3O_4@PPy, indicating that Au NPs were loaded on

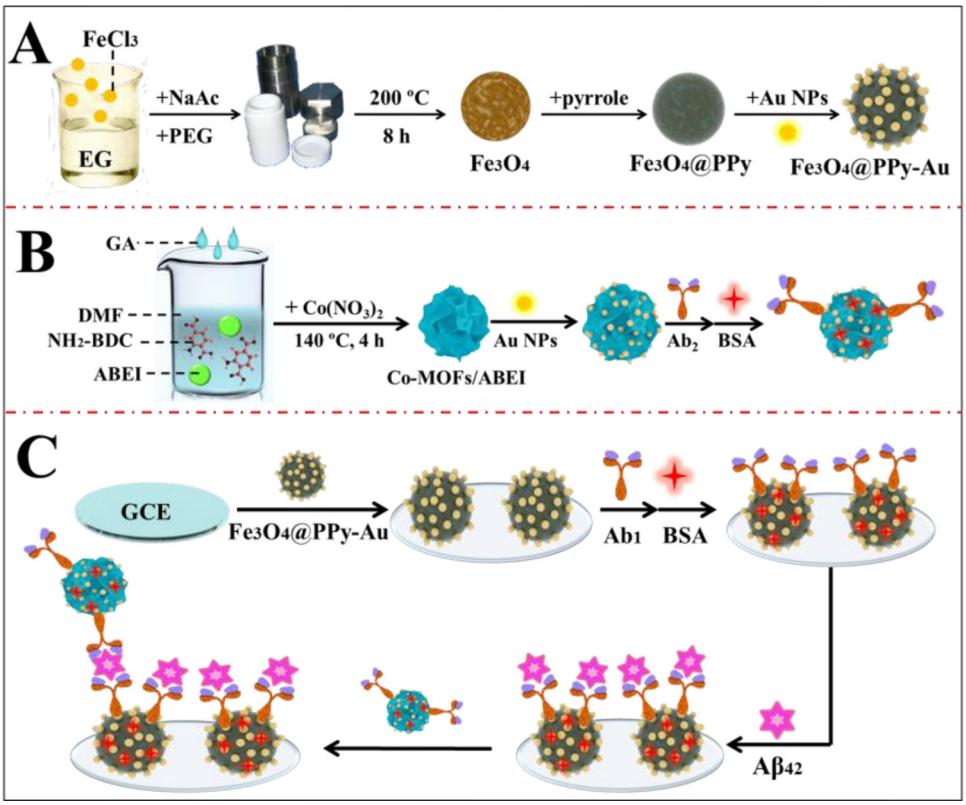

Scheme 1. Illustration for (A) the preparation process of Fe3O4@PPy-Au, (B) the preparation process of Co-MOFs/ABEI-Au, (C) the fabrication process of the Aβ42 immunosensor.

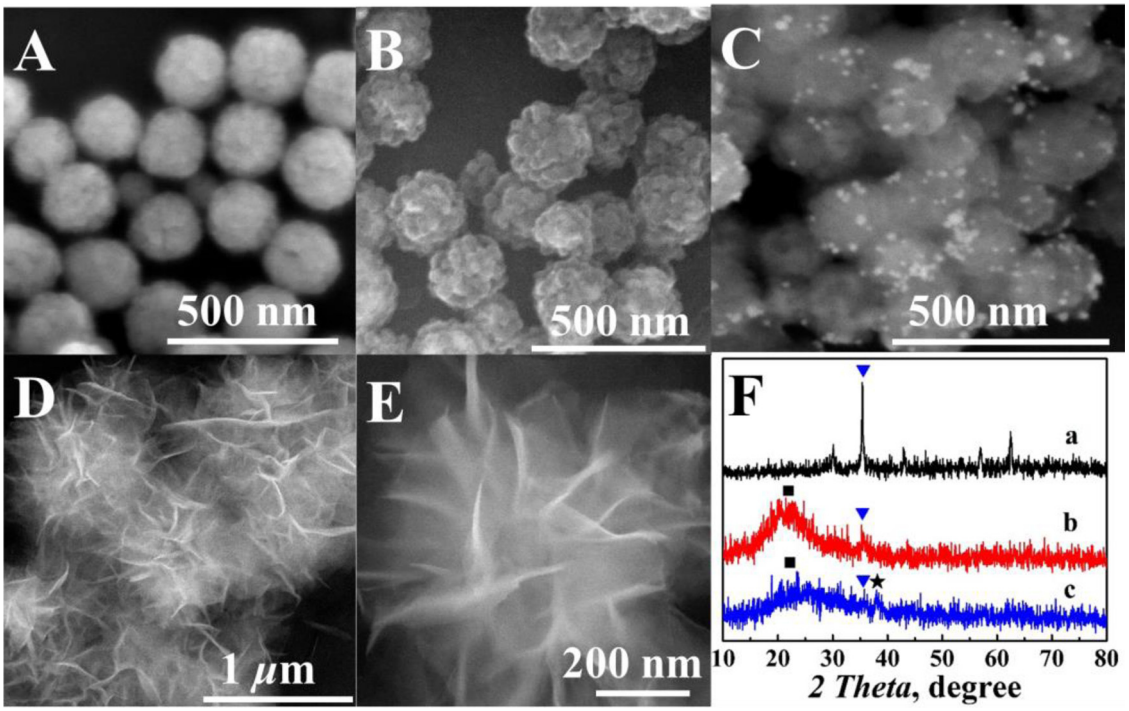

Fig. 1. SEM images of (A) Fe_3O_4, (B) Fe_3O_4@PPy, (C) Fe_3O_4@PPy-Au, (D) and (E) SEM images of Co-MOFs/ABEI at different dimensions, (F) the XRD image of Fe_3O_4 (a), Fe_3O_4@PPy (b) and Fe_3O_4@PPy-Au (c).

Fe_3O_4@PPy as expected. The SEM images of Co-MOFs/ABEI at different dimensions were displayed in Fig. 1D and E, from which a perfect flower-like structure with a uniform particle size distribution and an average diameter of 700 nm were observed clearly. The rough surface of Co-MOFs/ABEI could offer plenty of catalytic active sites for catalyzing the H_2O_2 decomposition. Besides, the powder X-ray diffraction (pXRD) of Fe_3O_4 (a), Fe_3O_4@PPy (b) and Fe_3O_4@PPy-Au (c) were also carried out and the results were displayed in Fig. 1F. The characteristic diffraction peaks of Fe_3O_4 at 2θ of 30.1°, 35.8°, 42.9°, 57.1° and 62.5° were derived from face-centered cubic lattice of Fe_3O_4 (JCPDS card no. 79-0418) [34]. As a conducting polymer, PPy was amorphous and exhibited a broad peak at 2θ of 20–30°. Meanwhile, the typical peaks of Fe_3O_4 were also observed in the XRD of Fe_3O_4@PPy nanocomposites [35]. In addition, the peak of Au at 2θ of 38.3° could be found from curve c, indicating that Au NPs were decorated on the surface of Fe_3O_4@PPy nanospheres. The pXRD results further revealed the successful preparation of Fe_3O_4@PPy-Au.

The elemental analysis and atom distribution of different materials were further investigated by energy dispersive X-ray spectroscopy (EDX), thermogravimetric analyzer (TGA) and transmission electron microscopy (TEM) mapping. Fig. 2A was the EDX of Fe_3O_4@PPy-Au which demonstrated the main elements of this nanomaterial containing C, N, O, Fe and Au. As displayed in Fig. 2B, the semi-quantitative elemental analysis of Co-MOFs/ABEI-Au using EDX exhibited the good distribution of C, N, O, Co, Au in the synthesized material with the weight percentage of 36.57, 5.34, 9.18, 0.45 and 48.06, respectively. The as-synthesized Co-MOFs/ABEI was also characterized by thermogravimetric analyzer (TGA), and the result was displayed in Fig. 2C. The first step with weight loss of 23.6% in the temperature range of 30–380 °C was ascribed to the removal of the adsorbed organic solvent and water inside in the pores of Co-MOFs/ABEI. The second step with weight loss of 28.2% happened between 380 °C and 500 °C, which was caused by the loss of organic ligands. The TEM mapping images with distinct color contrast for elements C, N, Co, Au were shown in Fig. 2D. A uniform distribution and high overlap of the elements can be observed clearly, which further verified the successful combination of Co-MOFs/ABEI and Au NPs.

The elemental composition of Co-MOFs/ABEI-Au was also inspected by X-ray photoelectron spectroscopy (XPS) and the results were presented in Fig. 3. As exhibited in Fig. 3A, the characteristic peaks of Au 4f, C 1s, N 1s, O 1s and Co 2p were observed distinctly from the wide scan survey spectra of Co-MOFs/ABEI-Au. As displayed in Fig. 3B, the doublet at 83.6 eV and 87.3 eV belongs to Au 4f, revealing that Au NPs were decorated on the surface of Co-MOFs/ABEI nanoflowers effectively. In the high resolution XPS spectra of C 1s (Fig. 3C), the peaks at 284.7, 285.7, 286.8, and 288.6 eV corresponded to the structures of C—C, C–N, C–O, and O—C═O, separately. The high resolution XPS spectra of N 1S (Fig. 3D) comprised two different peaks at 399.4 and 401.7 eV, corresponding to the structure of C-NH_2 and $-NR^{3+}/-NH^{3+}$. As demonstrated in Fig. 3F, the spectra of Co 2p possessed two main peaks with binding energies at around 783 and 798 eV, which were assigned to Co $2p_{3/2}$ and Co $2p_{1/2}$, respectively. The fitting peaks located at 778.6 and 794.9 eV for Co^{2+} species as well as 782.6 and 797.6 eV for Co^{3+} species were exhibited in Fig. 3F, implying the existence of both Co^{2+} and Co^{3+} in the Co-MOFs/ABEI-Au [36]. The shakeup satellite peaks of Co 2p (denoted as "sat.") and the peak area of each peak manifested that Co^{3+} was the majority of cobalt. The above XPS characterization results further proved the successful synthesis of Co-MOFs/ABEI-Au.

The UV–vis characterization of different materials was depicted in Fig. 4A. The typical absorption peaks of pure ABEI were located at 223 nm, 290 nm and 323 nm approximately, which was due to the UV absorption of $-NH_2$ group. The absorption peaks of Co-MOFs/ABEI showed a slight redshift, which was attributed to the larger π-bone-conjugation of ABEI crosslinked NH_2-BDC in Co-MOFs/ABEI. These results indicated that ABEI was immobilized on the Co-MOFs as anticipated. Besides, the ECL spectra of ABEI and Co-MOFs/ABEI were also acquired and depicted in Fig. 4B. The prepared Co-MOFs/ABEI nanomaterials displayed an obvious ECL peak at 450 nm (red curve), which was similar to that of pure ABEI (black curve), demonstrating that the prepared Co-MOFs/ABEI possessed the optical properties of ABEI and can be implemented in ECL analysis.

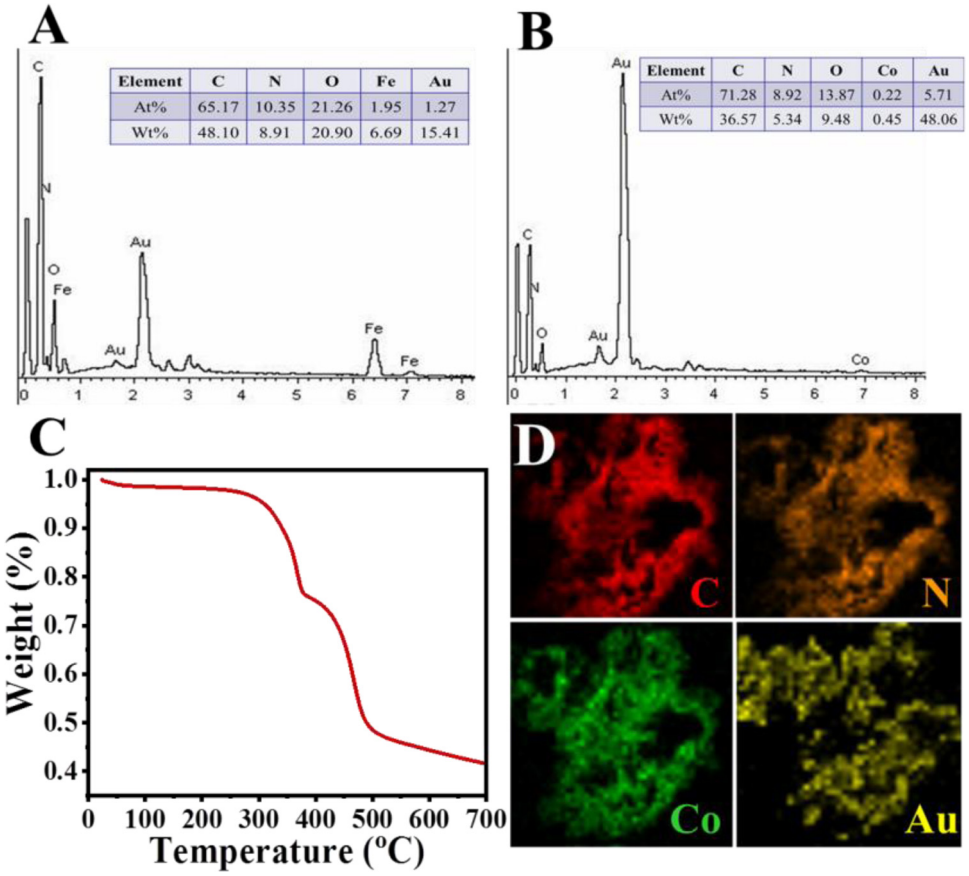

Fig. 2. (A) EDS of Fe_3O_4@PPy-Au, (B) EDS of Co-MOFs/ABEI-Au, (C) thermogravimetric analysis (TGA) curve of Co-MOFs/ABEI, (D) TEM element mapping images of C, N, Co, Au for Co-MOFs/ABEI-Au.

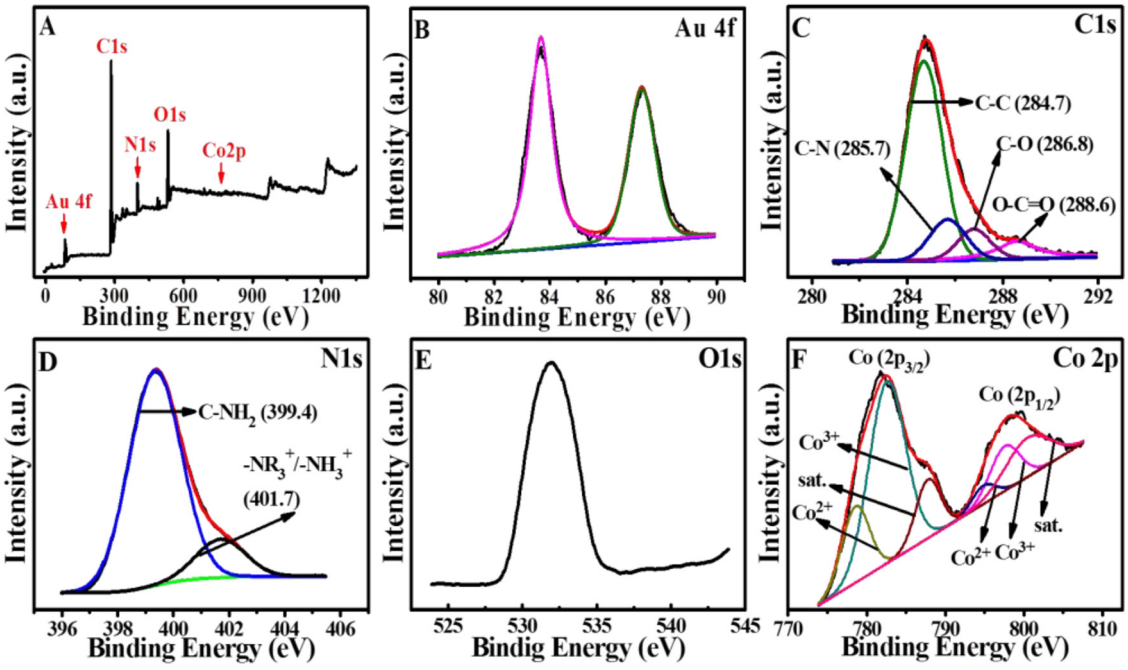

Fig. 3. XPS analysis for (A) the full region of Co-MOFs/ABEI-Au, (B) Au 4f region, (C) C 1s region, (D) N 1s region, (E) O1s region, and (F) Co 2p region.

3.2. Effects of Co-MOFs and Au NPs on the ECL intensity of ABEI

With the purpose of investigating positive effects of Co-MOFs and Au NPs on ECL enhancements of ABEI, contrast experiments were implemented through testing the ECL responses of different modified electrodes. The Co-MOFs solution was made by dispersing 5 mg of Co-MOFs into 1 mL of ultrapure water and the concentration of ABEI was 10 mM in the following experiments. As depicted in Fig. 4C, a weak ECL

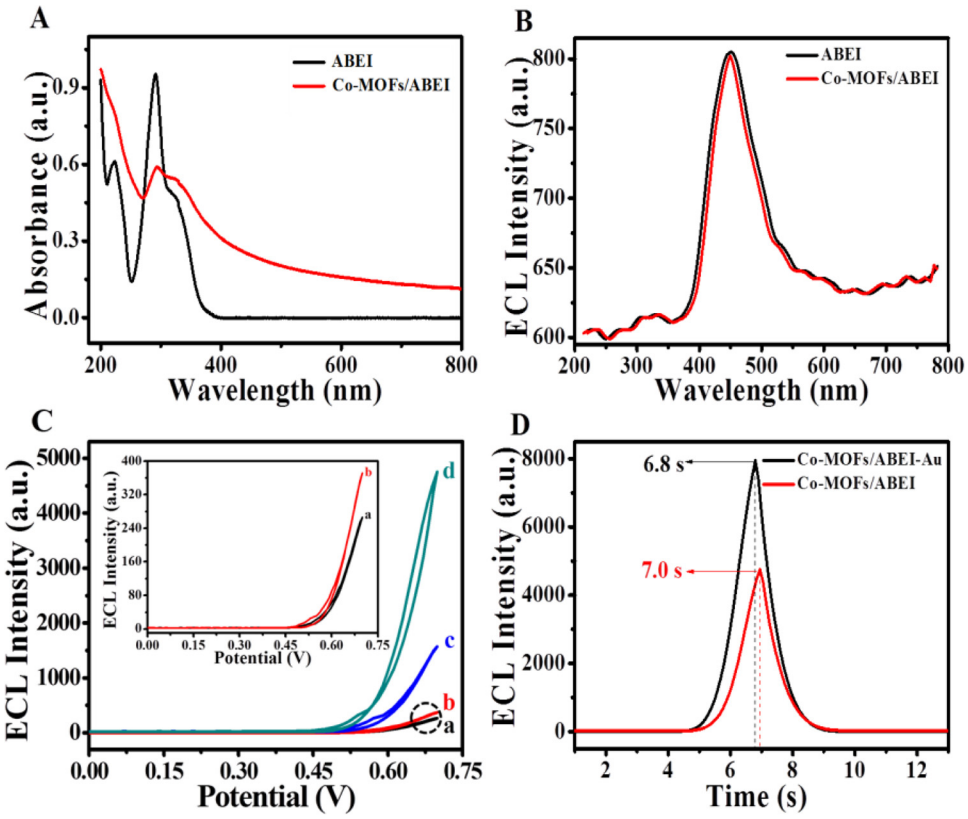

Fig. 4. (A) The UV–vis spectra of pure ABEI (black curve) and Co-MOFs/ABEI (red curve). (B) ECL spectra of ABEI (black curve) and Co-MOFs/ABEI (red curve). (C) ECL responses of bare GCE (curve a) and Co-MOFs/GCE (curve b) in 10 mL of PBS containing 10 μL of ABEI (10 mM), bare GCE (curve c) and Co-MOFs/GCE (curve d) in 10 mL of PBS containing 10 μL of H_2O_2 and 10 μL of ABEI (10 mM). (D) ECL intensity comparison of Co-MOFs/ABEI (red curve) and Co-MOFs/ABEI-Au modified immunosensor in 10 mL of PBS containing 10 μL of H_2O_2 (For interpretation of the references to colour in this figure legend, the reader is referred to the web version of this article).

signal about 400 a.u. was observed on the Co-MOFs modified electrode in 10 mL of PBS containing only 10 μL of ABEI (curve b), which was similar to that obtained from the bare electrode in PBS containing ABEI (curve a). Compared with the ECL response obtained from the bare electrode in PBS containing both ABEI and H_2O_2 (about 1574 a.u., curve c), the Co-MOFs modified electrode achieved a much stronger ECL response (about 4756 a.u., curve d) in the same condition, illustrating that Co-MOFs can enhance the ECL response of ABEI by accelerating the H_2O_2 decomposition into more reactive oxygen species (ROSs) on account of their desirable peroxidase mimics properties. This phenomenon could be ascribed to the existence of Co^{2+}/Co^{3+} redox pair and the quick conversion between Co^{2+} and Co^{3+} in the structure of Co-MOFs. It was reported that Co^{2+} ion could effectively catalyze the decompose process of H_2O_2, and the generated ROSs intermediates including superoxide radical and hydroxyl radical could oxidize ABEI to produce more excited state ABEI*, thus Co-MOFs were able to be robust co-reaction accelerators of H_2O_2 [37,38].

Furthermore, the influence of Au NPs on the ECL response of Co-MOFs/ABEI was explored. ECL signals generated from Co-MOFs/ABEI-Au-Ab_2 and Co-MOFs/ABEI-Ab_2 were recorded. It could be seen from Fig. 4D that ECL peak position of Co-MOFs/ABEI-Au-Ab_2 (black curve) appeared 0.2 s earlier in comparison of that of Co-MOFs/ABEI-Ab_2 (red curve), and a stronger ECL intensity was obtained with the assistance of Au NPs, which indicated the advance of Au NPs in facilating the electron transmission and boosting the ECL response of ABEI [39].

3.3. Electrochemical characterization of the fabricated immunosensor

Cyclic voltammetry (CV) and electrochemical impedance spectroscopy (EIS) were introduced to demonstrate the stepwise fabrication process of the immunosensor. The CV measurements were performed in 5 mM of $[Fe(CN)_6]^{4-/3-}$ containing 0.1 M of KCl. As presented in Fig. S1A, an apparent redox peaks of $[Fe(CN)_6]^{4-/3-}$ were observed in the pretreated electrode (curve a). After Fe_3O_4@PPy-Au was decorated on the surface of electrode, the peak current (curve b) decreased slightly for the relatively good conductivity and film-forming property of Fe_3O_4@PPy-Au (From the conductivity comparison of Fe_3O_4, Fe_3O_4@PPy and Fe_3O_4@PPy-Au, which was shown in the inset of Fig. S1A, we can see that after the Fe_3O_4 nanoparticle were wrapped by PPy and decorated with Au NPs, the conductivity of Fe_3O_4@PPy-Au was improved evidently). When the Fe_3O_4@PPy-Au/GCE was covered orderly with Ab_1, BSA and $Aβ_{42}$ antigen (Ag, 1 ng mL^{-1}), the related redox peak currents (curve c, d, and e) reduced in succession for the fact that these protein layers would hamper the electron transfer to a large extent.

Meanwhile, as another useful electrochemical measurement, EIS was performed to further confirm the assembly course of the immunosensor. The Nyquist plots of different modified electrodes as well as the equivalent circuit diagram were exhibited in Fig. S1B, and the corresponding data was displayed in Table S1. Among the impedance components of the solution resistance (R_s), the Warburg impedance (Z_w), the double layer capacitance (C_{dl}) and the charge transfer resistance (R_{et}), which were simulated with ZSimWin software, the R_{et} value was recognized as the most imperative index for it represented the obstructing behavior of the modified layers on the electrode surface [40]. As depicted in Fig. S1B, an almost straight line was acquired from the EIS curve of bare electrode (curve a), implying the small resistance value of the redox couple. After the modification of Fe_3O_4@PPy-Au, the EIS curve exhibited a small semicircle. Whereafter, consecutive increase of impedance values were obtained when Ab_1 (curve c) and BSA (curve d) were dripped on the electrode successively owing to the non-conductive character of protein molecules layers. The R_{et} kept increasing when $Aβ_{42}$ antigen was modified on the GCE (curve e), revealing that the immune complexes formed by $Aβ_{42}$ antigens and $Aβ_{42}$ antibodies hindered the electronic transmission between the electrochemical probe and electrode surface. The above EIS discussion was in accordance with the CV results.

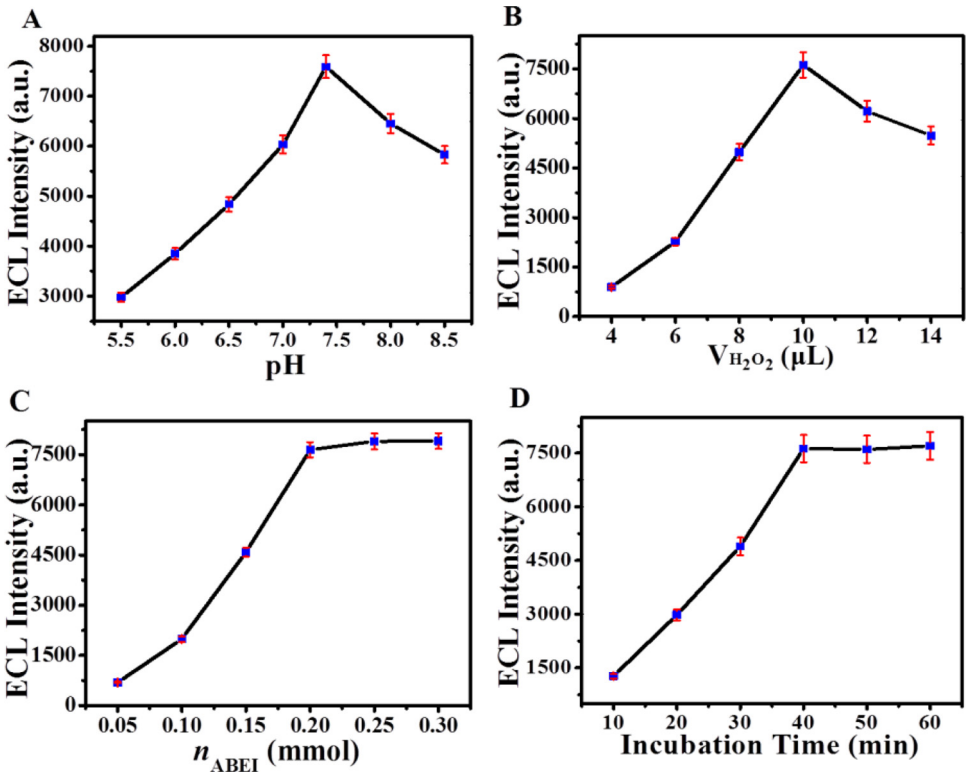

Fig. 5. Optimization of (A) the pH value of PBS, (B) the volume of H_2O_2, (C) the amount of ABEI, (D) the incubation time of Ab_2 bioconjugate.

3.4. Optimization of the experimental conditions

With the aim of realizing ultrasensitive detection of Aβ$_{42}$ antigen, experimental parameters including pH, the volume of H_2O_2, the amount of ABEI and the incubation time of Ab_2 bioconjugate were optimized. As seen from Fig. 5A, the effect of pH on the ECL responses was monitored in the range of 5.5–8.5. Clearly, the ECL signal enhanced as the pH of PBS varying from 5.5 to 7.4. With further increasing pH from 7.4 to 8.5, the ECL response declined gradually. This might be ascribed to that protein would denature or lose their effectiveness under overly acidic or alkaline circumstance, especially in alkalinity. The optimization experiment of H_2O_2 volume was conducted in 10 mL of PBS (pH 7.4). As clearly displayed in Fig. 5B, when the volume of H_2O_2 changed from 4 μL to 10 μL, a remarkable enhancement of ECL response was acquired. Consequently, 10 μL of H_2O_2 was used in the following research. More importantly, the amount of ABEI was another vital parameter regarding the performance of signal probe. As demonstrated in Fig. 5C, the ECL response got to the maximum value rapidly at 0.20 mmol and reached a plateau when the amount of ABEI exceeded 0.20 mmol. To avoid the waste of reagent, 0.20 mmol of ABEI was adopted during the preparation of Co-MOFs/ABEI. The influence of Ab_2 bioconjugate incubation time on the ECL signal was displayed in Fig. 5D. The ECL signal enhanced distinctly when the incubation time increased to 40 min in the case where stable immune complexes were formed by Ab_2 and Aβ$_{42}$ antigens. Thus, 40 min was chosen as the optimum incubation time.

3.5. Analytical performance of the proposed ECL immunosensor

Using Aβ$_{42}$ as a target analyte, the dependence of ECL intensity upon the concentration of Aβ$_{42}$ was assessed in 10 mL of PBS (pH 7.4) containing 10 μL of H_2O_2. From the results displayed in the inset of Fig. 6A, the ECL intensity increased accordingly as the concentrations of Aβ$_{42}$ varied from 10 fg mL^{-1} to 100 ng mL^{-1}. As exhibited in Fig. 6A, an excellent linear relationship between the ECL intensity and the logarithm of Aβ$_{42}$ concentration was achieved with a correlation coefficient of 0.99904 and a linear equation of $I = 7603.9 + 1368.7 \lg c$ (where I is the ECL intensity and c means the concentration of Aβ$_{42}$ (ng mL^{-1})). The limit of detection was figured to be 3 fg mL^{-1} (S/N = 3, the detailed calculation process was presented in Supplementary material). Importantly, in comparison with previous reports (Table 1), the fabricated ECL immunosensor demonstrated a satisfying performance with a lower detection limit, broader linear range as well as improved sensitivity, providing an attractive method for ultrasensitive detection of other biomarkers.

3.6. Related performance of the fabricated ECL immunosensor

Operational stability was considered to be a significant factor that influences the performance of immunosensors [46,47]. The operation stability of the immunosensor with different Aβ$_{42}$ concentrations was evaluated by continuous cyclic potential scans and the results were displayed in Fig. 6B. Clearly, there was no obvious change of the ECL response during three cycles scanning, suggesting the operational stability was acceptable. Meanwhile, the stability of long-term storage was also investigated by putting the modified electrode in a 4 °C freezer and detected every 5 days. According to Fig. 6C, no significant changes appeared in the ECL response after 20 days' storage with a relative standard deviation (RSD) of 4.81%, demonstrating the superb stability of the proposed immunosensor. From the practical view, the selectivity was another essential factor for the application of immunosensors [48]. Four kinds of possible interfering substances including carcino-embryonic antigen (CEA), prostate specific antigen (PSA), carbohydrate antigen 125 (CA125) and Aβ$_{40}$ with a concentration of 100 ng mL^{-1} was chosen to testify the selectivity of the immunosensor. As can be seen from Fig. 6D, negligible ECL responses were acquired from the interfering proteins CEA, PSA, CA125 and Aβ$_{40}$ incubated immunosensor. While the target Aβ$_{42}$ (1 ng mL^{-1}) and the mixed solution containing Aβ$_{42}$ (1 ng mL^{-1}) modified electrodes manifested strong ECL intensities even the concentration of target analyte was 100-fold

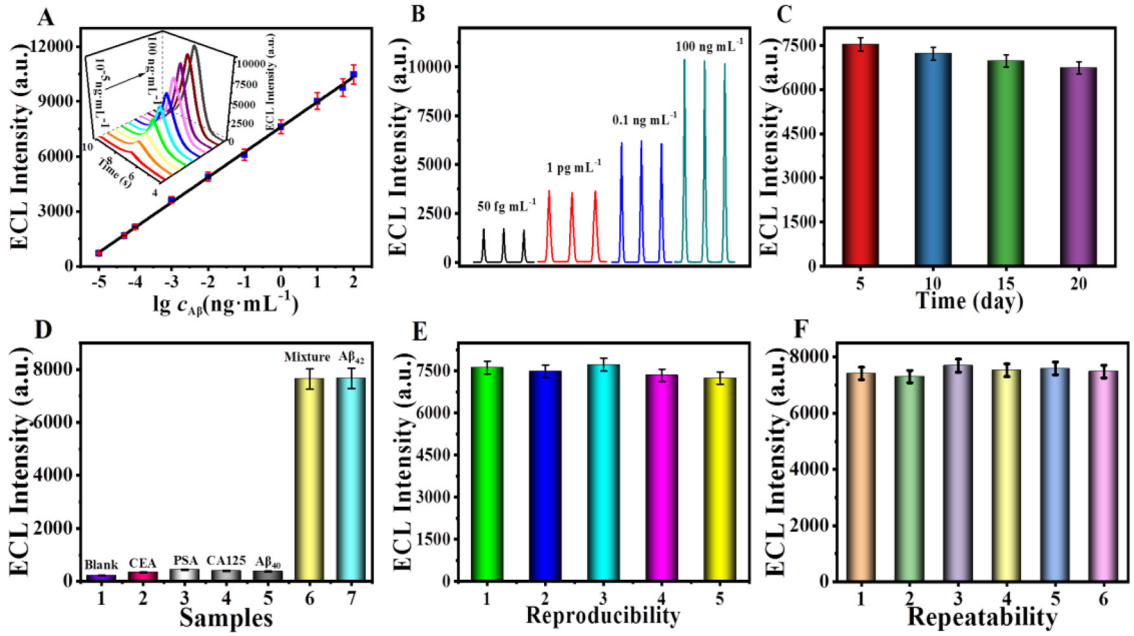

Fig. 6. (A) Calibration plots of the ECL intensity vs the logarithm of $A\beta_{42}$ concentration. (inset: ECL responses of the ECL immunosensor to different concentrations of $A\beta_{42}$: 0.00001, 0.00005, 0.0001, 0.001, 0.01, 0.1, 1, 10, 50, and 100 ng mL^{-1}.) (B) ECL stability of the proposed immunosensor to various concentrations of $A\beta_{42}$. (C) Long-term storage stability of the immunosensor incubated with 1 ng mL^{-1} of $A\beta_{42}$. (D) Selectivity of the proposed ECL immunosensor against different interfering substances: blank, 100 ng mL^{-1} of CEA, PSA, CA125, $A\beta_{40}$ and a mixture (containing 100 ng mL^{-1} of interfering substances and 1 ng mL^{-1} of $A\beta_{42}$). (E) Reproducibility of the proposed immunosensor with 1 ng mL^{-1} of $A\beta_{42}$ using five electrodes modified in the same condition. (F) Repeatability of the immunosensor by incubating the electrode with a controlled $A\beta_{42}$ concentration of 1 ng mL^{-1}.

lower than the interfering antigens, implying the satisfying selectivity of this immunoassay. The reproducibility of the immunoassay (Fig. 6E) was inspected meticulously through analysis of the same concentration of $A\beta_{42}$ (1 ng mL^{-1}) using five electrodes modified in the same condition. Semblable ECL intensities were achieved with the RSD of 2.64%, exhibiting a favorable reproducibility. Additionally, as shown in Fig. 6F, the repeatability of the immunosensor was estimated by incubating the electrode with a controlled $A\beta_{42}$ concentration of 1 ng mL^{-1}, and a relative standard deviation of 1.82% was obtained. The above results illustrated that the fabricated immunosensor with satisfying analytical performance could be applied to detect $A\beta_{42}$ in real samples.

3.7. Analysis of $A\beta_{42}$ in real samples

In order to identify the feasibility of this proposed immunoassay in Alzheimeir's disease diagnosis, standard addition method was adopted to carry out the recovery experiment. Firstly, three human serum samples were obtained from the Hospital of University of Jinan, and the original concentrations of $A\beta_{42}$ were detected to be 0.000023, 0.021, 17.2 ng mL^{-1}, respectively. Then, appropriate amounts of $A\beta_{42}$ standard solution (defined as Added) were added to the corresponding samples. With the same ECL response detection conducted five times, the corresponding concentrations of $A\beta_{42}$ (defined as Found) were calculated according to the obtained linear regression equation, and the average concentrations and recovery were figured out. As exhibited in Table S2, the recovery, which is defined as the ratio between the found concentration and the added concentration of $A\beta_{42}$, was in the range of 96.0%–104.0%, and the relative standard deviation (RSD) was within an acceptable range, demonstrating that the proposed immunosensor hold a great potential in clinical diagnosis of AD.

4. Conclusion

To summarize, an ultrasensitive ECL immunosensor for $A\beta_{42}$ determination was constructed in this work by means of synergistic catalysis of Co-MOFs and Au nanoparticles. This work has brought forth the following novel ideas. Primarily, ABEI not only served as an ECL luminophore, but also played the role of reductant in the synthesis of Co-MOFs. The obtained Co-MOFs/ABEI overcame the limitation of finite ABEI loading capacity and cumbersome preparation process caused by the traditional immobilization methods of ABEI, realized the abundantly loading of ABEI and ECL signal boosting. More importantly, the flower-like Co-MOFs with intrinsic peroxidase mimic property were employed as co-reaction accelerators to speed up the decomposition of H_2O_2 for more ROSs generation, which were conducive to produce more excited state ABEI*. Meanwhile, Au nanoparticles were decorated on the Co-MOFs/ABEI via electrostatics attraction, leading to the

Table 1
Comparison of our work with previous works for $A\beta_{42}$ detection.

Method	Detection range	Detection limit	References
Electrochemical	10 pg mL^{-1}–1 ng mL^{-1}	5.2 pg mL^{-1}	[5]
Photoelectrochemical	0.5 pg mL^{-1}–100 ng mL^{-1}	0.17 pg mL^{-1}	[41]
Electrochemiluminescence	100 fg mL^{-1}–10 ng mL^{-1}	19.95 fg mL^{-1}	[42]
Electrochemiluminescence	80 fg mL^{-1}–100 ng mL^{-1}	5.2 fg mL^{-1}	[43]
Electrochemical	0.1 pg mL^{-1}–100 ng mL^{-1}	30 fg mL^{-1}	[44]
Colorimeric	7.5 nM–350 nM	2.3 nM	[45]
Electrochemiluminescence	10 fg mL^{-1}–100 ng mL^{-1}	3 fg mL^{-1}	This work

amplification of ECL response. Moreover, Fe_3O_4@PPy-Au nanoparticles with large specific surface area and admirable biocompatibility were chosen as the sensing platform for the capture antibodies immobilization. The fabricated sandwiched ECL immunosensor exhibited a sensitive response to $A\beta_{42}$ with a linear range of 10 fg mL^{-1}–100 ng mL^{-1} and a low detection limit of 3 fg mL^{-1}. Featuring excellent sensitivity and selectivity, this work not only offered a newfangled method to synthesize ABEI derivative with high luminous efficiency, but also provided a reliable and effective strategy for $A\beta_{42}$ detection and Alzheimer's disease diagnosis in clinical application.

Acknowledgments

This work was supported by the National Key Scientific Instrument and Equipment Development Project of China (No. 21627809), and the National Natural Science Foundation of China (No. 21575050 and No. 21505051).

Appendix A. Supplementary data

Supplementary material related to this article can be found, in the online version, at doi:https://doi.org/10.1016/j.snb.2019.04.097.

References

[1] K. Hegnerová, M. Bocková, H. Vaisocherová, Z. Krištofiková, J. Říčný, D. Řípová, et al., Surface plasmon resonance biosensors for detection of Alzheimer disease biomarker, Sens. Actuators B: Chem. 139 (2009) 69–73.
[2] Q. Jieling, P.J. Su, J.D. Gyu, C. Misuk, L. Youngkwan, Curcumin-based electrochemical sensor of amyloid-β oligomer for the early detection of Alzheimer's disease, Sens. Actuators B: Chem. 273 (2018) 1593–1599.
[3] J.V. Rushworth, A. Ahmed, H.H. Griffiths, N.M. Pollock, N.M. Hooper, P.A. Millner, A label-free electrical impedimetric biosensor for the specific detection of Alzheimer's amyloid-beta oligomers, Biosens. Bioelectron. 56 (2014) 83–90.
[4] P. Gagni, L. Sola, M. Cretich, M. Chiari, Development of a high-sensitivity immunoassay for amyloid-beta 1–42 using a silicon microarray platform, Biosens. Bioelectron. 47 (2013) 490–495.
[5] P. Carneiro, J. Loureiro, C. Delerue-Matos, S. Morais, M.D.C. Pereira, Alzheimer's disease: development of a sensitive label-free electrochemical immunosensor for detection of amyloid beta peptide, Sens. Actuators B: Chem. 239 (2017) 157–165.
[6] N. Xia, B. Zhou, N. Huang, M. Jiang, J. Zhang, L. Liu, Visual and fluorescent assays for selective detection of beta-amyloid oligomers based on the inner filter effect of gold nanoparticles on the fluorescence of CdTe quantum dots, Biosens. Bioelectron. 85 (2016) 625–632.
[7] L. Liu, Q. He, F. Zhao, N. Xia, H. Liu, S. Li, et al., Competitive electrochemical immunoassay for detection of β-amyloid (1–42) and total β-amyloid peptides using p-aminophenol redox cycling, Biosens. Bioelectron. 51 (2014) 208–212.
[8] R. Xu, D. Wei, B. Du, W. Cao, D. Fan, Y. Zhang, et al., A photoelectrochemical sensor for highly sensitive detection of amyloid beta based on sensitization of Mn:CdSe to Bi_2WO_6/CdS, Biosens. Bioelectron. 122 (2018) 37–42.
[9] M.K. Kang, J. Lee, A.H. Nguyen, S.J. Sim, Label-free detection of ApoE4-mediated β-amyloid aggregation on single nanoparticle uncovering Alzheimer's disease, Biosens. Bioelectron. 72 (2015) 197–204.
[10] L. Li, Y. Chen, J.J. Zhu, Recent advances in electrochemiluminescence analysis, Anal. Chem. 89 (2016) 358–371.
[11] L. Yang, Y. Li, Y. Zhang, D. Fan, X. Pang, Q. Wei, et al., 3D nanostructured Palladium-functionalized graphene-aerogel-supported Fe_3O_4 for enhanced Ru $(bpy)_3^{2+}$-based electrochemiluminescent immunosensing of prostate specific antigen, ACS Appl. Mater. Interfaces 9 (2017) 35260–35267.
[12] X. Huang, X. Deng, W. Qi, D. Wu, Highly sensitive luminol electrochemiluminescence immunosensor based on platinum-gold alloy hybrid functionalized zinc oxide nanocomposites for catalytic amplification, Sens. Actuators B: Chem. 273 (2018) 466–472.
[13] B. Xing, W. Zhu, X. Zheng, Y. Zhu, Q. Wei, D. Wu, Electrochemiluminescence immunosensor based on quenching effect of SiO_2@PDA on SnO_2/rGO/Au NPs-luminol for insulin detection, Sens. Actuators B: Chem. 265 (2018) 403–411.
[14] X. Xie, H. Wang, L. Zhang, Y. Liu, Y. Chai, Y. Yuan, et al., A novel electrochemiluminescence immunosensor based on functional β-cyclodextrin-ferrocene host-guest complex with multiple signal amplification, Sens. Actuators B: Chem. 258 (2018) 1146–1151.
[15] Y. Yu, H. Zhang, Y. Chai, R. Yuan, Y. Zhuo, A sensitive electrochemiluminescent aptasensor based on perylene derivatives as a novel co-reaction accelerator for signal amplification, Biosens. Bioelectron. 85 (2016) 8–15.
[16] J. Zhao, W. Liang, Y. Lei, Y. Ou, Y. Chai, R. Yuan, et al., An efficient electrochemiluminescence amplification strategy via bis-co-reaction accelerator for sensitive detection of laminin to monitor overnutrition associated liver damage, Biosens. Bioelectron. 98 (2017) 317–324.
[17] M.Y. Emran, S.A. El-Safty, M.A. Shenashen, T. Minowa, A well-thought-out sensory protocol for screening of oxygen reactive species released from cancer cells, Sens. Actuators B: Chem. 284 (2019) 456–467.
[18] S. Li, Z. Liu, J. Li, A. Chen, Y. Chai, R. Yuan, et al., Enzyme-free target recycling and double-output amplification system for electrochemiluminescent assay of mucin 1 with MoS_2 nanoflowers as co-reaction accelerator, ACS Appl. Mater. Interfaces 10 (2018) 14483–14490.
[19] Z. Liu, S. Li, R. Wei, A. Chen, Y. Chai, R. Yuan, et al., CuS porous nanospheres as a novel noble metal-free co-reaction accelerator for enhancing electrochemiluminescence and sensitive immunoassay of mucin 1, Sens. Actuators B: Chem. 274 (2018) 110–115.
[20] F. Yang, X. Jiang, X. Zhong, S. Wei, R. Yuan, Highly sensitive electrochemiluminescence detection of mucin1 based on V_2O_5 nanospheres as peroxidase mimetics to catalyze H_2O_2 for signal amplification, Sens. Actuators B: Chem. 265 (2018) 126–133.
[21] I.M. El-Sewify, M.A. Shenashen, A. Shahat, H. Yamaguchi, M.M. Selim, M.M.H. Khalil, et al., Dual colorimetric and fluorometric monitoring of Bi^{3+} ions in water using supermicroporous Zr-MOFs chemosensors, J. Lumin. 198 (2018) 438–448.
[22] I.M. El-Sewify, M.A. Shenashen, A. Shahat, M.M. Selim, M.M.H. Khalil, S.A. El-Safty, Sensitive and selective fluorometric determination and monitoring of Zn^{2+} ions using supermicroporous Zr-MOFs chemosensors, Microchem. J. 139 (2018) 24–33.
[23] C. Xiong, W. Liang, Y. Zheng, Y. Zhuo, Y. Chai, R. Yuan, Ultrasensitive assay for telomerase activity via self-enhanced electrochemiluminescent ruthenium complex doped metal-organic frameworks with high emission efficiency, Anal. Chem. 89 (2017) 3222–3227.
[24] X. Dong, G. Zhao, L. Liu, X. Li, Q. Wei, W. Cao, Ultrasensitive competitive method-based electrochemiluminescence immunosensor for diethylstilbestrol detection based on $Ru(bpy)_3^{2+}$ as luminophor encapsulated in metal-organic frameworks UiO-67, Biosens. Bioelectron. 110 (2018) 201–206.
[25] X. Jiang, Z. Wang, H. Wang, Y. Zhuo, R. Yuan, Y. Chai, A novel metal-organic framework loaded with abundant N-(aminobutyl)-N-(ethylisoluminol) as a high-efficiency electrochemiluminescence indicator for sensitive detection of mucin1 on cancer cells, Chem. Commun. (2017) 9705–9708.
[26] X. Yang, J. Lv, Z. Yang, R. Yuan, Y.Q. Chai, A sensitive electrochemical aptasensor for thrombin detection based on electroactive co-based metal-organic frameworks with target-triggering NESA strategy, Anal. Chem. 89 (2017) 11636–11640.
[27] M.Y. Emran, M.A. Shenashen, M. Mekawy, A.M. Azzam, N. Akhtar, H. Gomaa, et al., Ultrasensitive in-vitro monitoring of monoamine neurotransmitters from dopaminergic cells, Sens. Actuators B: Chem. 259 (2018) 114–124.
[28] Mohammed Y. Emran, M. Mekawy, N. Akhtar, Mohamed A. Shenashen, Islam M. El-Sewify, A. Faheem, et al., Broccoli-shaped biosensor hierarchy for electrochemical screening of noradrenaline in living cells, Biosens. Bioelectron. 100 (2018) 122–131.
[29] M.Y. Emran, M.A. Shenashen, A.A. Abdelwahab, H. Khalifa, M. Mekawy, N. Akhtar, et al., Design of hierarchical electrocatalytic mediator for one step, selective screening of biomolecules in biological fluid samples, J. Appl. Electrochem. 48 (2018) 529–542.
[30] M. Emran, M. Shenashen, H. Morita, S. El-Safty, 3D-ridge stocked layers of nitrogen-doped mesoporous carbon nanosheets for ultrasensitive monitoring of dopamine released from PC12 cells under K^+ stimulation, Adv. Healthc. Mater. (2018) 1701459–1701469.
[31] M.Y. Emran, M.A. Shenashen, H. Morita, S.A. El-Safty, One-step selective screening of bioactive molecules in living cells using sulfur-doped microporous carbon, Biosens. Bioelectron. 109 (2018) 237–245.
[32] M.Y. Emran, M. Shenashen, A.A. Abdelwahab, M. Abdelmottaleb, S. El-Safty, Facile synthesis of microporous sulfur-doped carbon spheres as electrodes for ultrasensitive detection of ascorbic acid in food and pharmaceutical products, New J. Chem. 42 (2018) 5037–5044.
[33] Y. Wang, B. Zou, T. Gao, X. Wu, S. Lou, S. Zhou, Synthesis of orange-like Fe_3O_4/PPy composite microspheres and their excellent Cr(VI) ion removal properties, J. Mater. Chem. 22 (2012) 9034–9040.
[34] Z. Hui, Z. Xue, X. Jing-Juan, C. Hong-Yuan, Fe_3O_4/polypyrrole/Au nanocomposites with core/shell/shell structure: synthesis, characterization, and their electrochemical properties, Langmuir 24 (2008) 13748–13752.
[35] K. Cheah, M. Forsyth, V.T. Truong, Ordering and stability in conducting polypyrrole, Synth. Met. 94 (1998) 215–219.
[36] Y. Fan, Y. Ji, G. Zheng, J. Lu, D. Kong, X. Yin, et al., Degradation of atrazine in heterogeneous Co_3O_4 activated peroxymonosulfate oxidation process: kinetics, mechanisms, and reaction pathways, Chem. Eng. J. 330 (2017) 831–839.
[37] L.L. Klopf, T.A. Nieman, Effect of iron(II), cobalt(II), copper(II), and manganese(II) on the chemiluminescence of luminol in the absence of hydrogen peroxide, Anal. Chem. 55 (1983) 1080–1083.
[38] X. Jiang, H. Wang, H. Wang, Y. Zhuo, R. Yuan, Y. Chai, Electrochemiluminescence biosensor based on 3-D DNA nanomachine signal probe powered by protein-aptamer binding complex for ultrasensitive mucin 1 detection, Anal. Chem. 89 (2017) 4280–4286.
[39] H. Chu, W. Guo, J. Di, W. Ying, Y. Tu, Study on sensitization from reactive oxygen species for electrochemiluminescence of luminol in neutral medium, Electroanalysis 21 (2010) 1630–1635.
[40] D. Wu, Y. Wei, X. Ren, X. Ji, Y. Liu, X. Guo, et al., $Co(OH)_2$ nanoparticle-encapsulating conductive nanowires array: room-temperature electrochemical preparation for high-performance water oxidation electrocatalysis, Adv. Mater. 30 (2018) 1705366–1705372.
[41] Y. Wang, D. Fan, G. Zhao, J. Feng, D. Wei, N. Zhang, et al., Ultrasensitive photoelectrochemical immunosensor for the detection of amyloid β-protein based on

$SnO_2/SnS_2/Ag_2S$ nanocomposites, Biosens. Bioelectron. 120 (2018) 1–7.
[42] Y. Jia, L. Yang, R. Feng, H. Ma, D. Fan, T. Yan, et al., $MnCO_3$ as a new electrochemiluminescence emitter for ultrasensitive bioanalysis of β-$Amyloid_{1-42}$ oligomers based on site-directed immobilization of antibody, ACS Appl. Mater. Interfaces 11 (2019) 7157–7163.
[43] J.X. Wang, Y. Zhuo, Y. Zhou, H.J. Wang, R. Yuan, Y.Q. Chai, Ceria doped zinc oxide nanoflowers enhanced luminol-based electrochemiluminescence immunosensor for Amyloid-β detection, ACS Appl. Mater. Interfaces 8 (2016) 12968–12975.
[44] J. Han, M. Zhang, G. Chen, Y. Zhang, Q. Wei, Y. Zhuo, et al., Ferrocene covalent-confined in porous MOF as signal tags for highly sensitive electrochemical immunoassay of amyloid-β, J. Mater. Chem. B 5 (2017) 8330–8336.
[45] T. Hu, S. Lu, C. Chen, J. Sun, X. Yang, Colorimetric sandwich immunosensor for Aβ1-42 based on dual antibody-modified gold nanoparticles, Sens. Actuators B: Chem. 243 (2017) 792–799.
[46] H. Ma, Y. Zhao, Y. Liu, Y. Zhang, D. Wu, H. Li, et al., A compatible sensitivity enhancement strategy for electrochemiluminescence immunosensors based on the biomimetic melanin-like deposition, Anal. Chem. 89 (2017) 13049–13053.
[47] L. Yang, W. Zhu, X. Ren, M.S. Khan, Y. Zhang, B. Du, et al., Macroporous graphene capped Fe_3O_4 for amplified electrochemiluminescence immunosensing of carcinoembryonic antigen detection based on CeO_2@TiO_2, Biosens. Bioelectron. 91 (2017) 842–848.
[48] X. Ren, H. Ma, T. Zhang, Y. Zhang, T. Yan, B. Du, et al., Sulfur-doped graphene-based immunological biosensing platform for multianalysis of cancer biomarkers, ACS Appl. Mater. Interfaces 9 (2017) 37637–37644.

Chao Wang studies in school of chemistry and chemical engineering, University of Jinan as a postgraduate student. She is working on designing electrochemiluminescence sensors.

Nuo Zhang received her B.S. degree in biological technology from University of Jinan in 2007 and M.S. degree in analytical chemistry from University of Jinan in 2010. Now, she is a lecturer at University of Jinan. Her main research interests are electrochemical biosensors and photoelectrochemical biosensors.

Yueyuan Li is a current master student, studies in school of chemistry and chemical engineering, University of Jinan. She is working on constructing electrochemical sensors.

Lei Yang studies in school of chemistry and chemical engineering, University of Jinan as a postgraduate student. He is working on constructing electrochemiluminescence sensors.

Dong Wei received his Ph.D. degree from Shandong University, Shandong, China. His research interests focus on wastewater treatment.

Tao Yan received the Ph.D. degree from Beijing Institute of Technology (BIT), Beijing, China. He is an associate professor of school of resource and environment at University of Jinan, Shandong, China. His research interests focus on the construction of photoelectric functional materials for biosensor, energy and environment applications.

Huangxian Ju received his BS, MS and Ph.D. degrees from Nanjing University during 1982–1992. He was a postdoc in Montreal University (Canada) from 1996 to 1997 and a guest professor in three universities of Germany and Ireland in 1999-2000. He became an associate and full professor of Nanjing University in 1993 and 1999. He is currently the director of State Key Laboratory of Analytical Chemistry for Life Science. His research interests focus on analytical biochemistry, biosensing and molecular diagnosis. He has published 616 papers in different journals with SCI h-index of 83 (29,523 citations) and Google Scholar h-index of 91 with more than 29,000 citations.

Bin Du, a professor and doctoral supervisor, has been engaged in analytic chemistry and environmental science research for many years. He acquired the degree of doctor of science from Chinese Academy of Sciences. He has been investigating deeply on the composition, property and application of micro emulsion.

Qin Wei, a professor and DSc, has devoted herself to analytical teaching and scientific research. Her main research interests are the determination of protein and nucleic acid by photometry and the electrochemical immunosensor preparation. She has published over one hundred articles on analysis, immunosensor and applied successfully for many research projects, such as *Biomaterials, Adv. Funct. Mater., Biosens. Bioelectron., Sens. Actuators B: Chem., Talanta.*